Integration of Diffractive Optics for Top-Hat Generation and Enhanced Depth of Focus

Christian Bischoff[*1,2], Ulrich Rädel[1], Udo Umhofer[1], Erwin Jäger[1], and Andrés Fabián Lasagni[2,3]

[1]*Topag Lasertechnik GmbH, Nieder-Ramstädter Str. 247, 64285 Darmstadt, Germany*
[2]*Institut für Fertigungstechnik, Technische Universität Dresden, George-Bähr-Str. 3c, 01069 Dresden, Germany*
[3]*Fraunhofer-Institut für Werkstoff- und Strahltechnik IWS, Winterbergstr. 28, 01277 Dresden, Germany*
[*]*Corresponding author's e-mail: bischoff@topag.de*

Diffractive optics can be used to generate Top-Hat profiles in the working plane. In addition, there are theoretical considerations to use such concepts to increase the depth of field of a Gaussian laser beam. Within the scope of this work, we show the theoretical propagation behavior through free space behind a diffractive optic and relate characteristic propagation effects to the Rayleigh length zr of the initial beam used. It will be shown that Top-Hat profiles can be generated without any focusing power. From the knowledge gained from theoretical free space propagation calculation, we derive instructions as to what needs to be considered when combining the diffractive elements with focusing systems to realize an increased depth of field and how the size of Top-Hat profiles behind a focusing optic can be influenced. Furthermore, experiments results will be presented that demonstrate the propagation behavior in free space, a possible adjustment of Top-Hat size and the increase of the depth of field of a Gaussian laser beam.

1. Introduction

Pulsed laser systems with pulse durations in the nanosecond (short pulse), picosecond or femtosecond (ultrashort pulse) range are used for a large number of applications today [1-7]. Such systems typically deliver pulses with a TEM_{00} Gaussian beam profile, high beam quality and pulse energies of a few 100 µJ.

A Gaussian light distribution is the desired spatial intensity profile for many applications because it maintains its distribution during propagation and focusing. It enables excellent focusing to a few microns, resulting in high structural resolution of the laser micromachining process. However, in recent years it has been shown that light distributions adapted to the process, such as multi-beam arrays, Top-Hat profiles or Bessel beams, are advantageous for a large number of applications. [8-16]

These adjustments of the light distribution are made by optical elements that shape the beam. These are typically non-absorbing optical components that allow targeted changes in the phase information of the complex wave field of the Gaussian beam. A change in the amplitude would be accompanied by absorption, which would lead to undesirable effects when used in the high-power range. The changed wave field is then focused. The focusing optic acts as a Fourier transformer [17]. The desired intensity distribution in the processing plane can thus be determined in advance by means of Fourier transformation of the complex wave field modified by the beam-shaping optic.

Various calculation methods are used to calculate the phase information. For example, continuous surfaces for refractive beam shapers are often calculated using mapping methods [18, 19]. The intensity distributions that can be realized by means of such optics typically have a continuous profile. They are therefore often used to create Top-Hat or Donut profiles. The advantage of such surface profiles lies in the highest efficiency, but the achievable light distributions are limited.

A completely opposite method uses highly irregular structures, similar to a chessboard pattern in which the black and white fields are randomly distributed. White areas are raised by a few 100 nm compared to black areas. The lateral structure size of the individual fields is in the range from one to a few micrometers. The function of such optics is based on the principle of diffraction, which occurs on the micro structured surface of these elements. Due to the almost freely selectable surface structures, almost any light distribution can be generated with an appropriate design. Iterative methods are typically used for the design of such structures, such as those required to generate a dot matrix for beam splitting. Many are based on the so-called Iterative Fourier Transform Algorithm (IFTA) [20 -22]. The disadvantage of such elements is often the low efficiency [23] and the formation of speckles [24].

Various techniques are used to impress the determined phase information on the laser beam. These techniques can be divided into dynamic and static variants. Dynamic vari-

ants include deformable mirrors (DM) or liquid crystal spatial light modulators (SLM). These can flexibly influence the phase. Refractive as well as diffractive phase information are possible, which means that almost any light distribution can be adapted to the respective task. A disadvantage, however, is that they typically only tolerate a few watts of average power [25]. Nevertheless, SLMs in particular are now also being used in material processing with ultrashort pulse lasers [8, 9].

In contrast to this, optics made of quartz glass provide static phase information and thus light distribution. They have a significantly higher radiation resistance and are many times cheaper than the dynamic methods. Continuous refractive surfaces with a rotationally symmetrical profile, like aspheres or cylindrical optics are typically produced by means of a grinding process. Surfaces with non-rotationally symmetrical profiles allow the generation of profiles with non-rotationally footprint. Such so-called free-form optics can be produced using ultra precision manufacturing [26] or plasma processing [27]. To produce diffractive optical elements, lithographic processes from semiconductor technology are used, such as Reactive-Ion-Etching (RIE) or Ion-Beam-Etching (IBE) [28 – 30].

One diffractive beam shaping method is the so-called FBS® concept [31]. This allows the generation of diffraction limited speckles free Top-Hat profiles and has been shown to be advantageous for Laser-Induced Breakdown Spectroscopy (LIBS) [32, 33], Matrix-assisted Laser Desorption/Ionization (MALDI) [34], Direct Laser Interference Patterning (DLIP) [35] and thin film applications [36, 37]. In addition, there are theoretical considerations to use this concept to increase the depth of field of a Gaussian laser beam [38].

In the context of this work, the free space propagation of the shaped beam is investigated. From the findings of the theoretical free space propagation calculation, information is derived as to what needs to be considered when integrating these diffractive optics in order to achieve an increased depth of field and how the position and size of the achievable Top-Hat profiles are influenced. In addition, it is shown how the variability of beam shaping can be increased by adapting the optical setup. The results of the experiments confirm the theoretical considerations.

2. Mathematical considerations
2.1 Feature for Top-Hat generation
All results shown here originate from the diffractive FBS® beam shaping concept. The diffractive structure is illuminated with a Gaussian beam. The amplitude g(x,y) of a Gaussian beam is given by [39]:

$$g\left(x,y\right) = exp\left(-\frac{x^2+y^2}{\omega^2}\right) \qquad (1)$$

There is a scaling factor s of the diffractive structure that determines the optical function of the element. With s=ω, a Top-Hat profile, with a square footprint is obtained in the focal plane.

2.2 Setup of simulations
The beam shaping concept is based on diffraction of coherent light. For the simulation of the propagation behavior of unfocused and focused beams, the commercial physical optics software VirtualLab Fusion was used, on a workstation with an AMD Ryzen™ Threadripper™ 2990WX processor, 32 cores, 3GHz and 128GB RAM memory. VirtualLab Fusion provides two physical optics simulation engines, Classical Field Tracing and Field Tracing 2nd Generation. In this study Field Tracing 2nd Generation was used, which selects automatically the most suitable Fourier transform out of Fast Fourier Transformation, Semi-Analytical Fourier Transformation and Homeomorphic Fourier Transformation [40, 41].

The laser beam used was Gaussian, TEM_{00} and had an ideal beam quality of $M^2= 1$. With a view to ultra-short pulse laser material processing, this approach is justified, since beams with almost ideal beam quality are typically used here. In addition, aberration-free optical systems are assumed. This is permissible with regard to the experiments shown, since our own optical systems were set up and qualified. The extent to which the results shown here can be transferred to beams with a significantly poorer beam profile and to optical systems afflicted with imaging errors must be investigated in further work.

2.3 Generation of caustics
In this work calculated caustics of unfocused and focused beams are presented. To generate the caustics several cross-sections of the intensity profile along the x-axis are calculated at different positions along the propagation axis z (optical axis) and stringed together. It is also assumed, that for each z position the cross-sections of the y –axis is equal to the cross-sections of the x –axis. Each displayed image of a calculated caustic is normalized to the individual maximum intensity.

3. Results and discussion
3.1 Simulation results
The aim of the simulations carried out is to get an overview of which parameters influence the caustic of focused shaped beams and therefore the beam shaping result for Top-Hat generation. Further it is investigated, how beam shaping can increase the depth of field and to what extent. There is also the idea to generate homogenized profiles with different geometries, not just square ones.

The investigations in this work will show that in order to properly understand why the caustics of a shaped beam changes under certain circumstances, one at first has to deal with the propagation of the shaped, unfocused beam in free space. For this reason, free space propagation is dealt with first. The knowledge gained will help in the following sections to understand the conditions for a successful integration of the beam shaper into the beam path.

3.1.1 Free space propagation of shaped beam
In order to understand the conditions that have to be considered when integrating the beam shaping elements into beam paths, one must first deal with the propagation behavior of the shaped beam in free-space. Figure 1 shows the setup used in this section in the simulations with the parameters ω_{fs}=s, a and b. ω_{fs} designates the beam radius in the waist of the Gaussian beam in free-space. The waist describes the smallest spatial extension of ω of the Gaussian beam. Parameter a designates the distance between the waist

and the beam shaper and b the distance between the beam shaper and the detection plane.
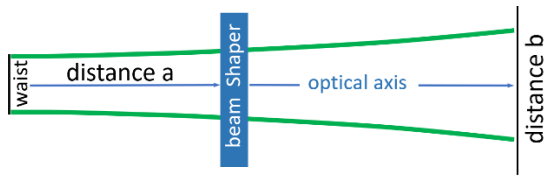

Fig. 1 Simulation setup for free space propagation

In order to be able to better recognize the change in caustic that occurs when the beam shaping element is introduced into the beam path, the well-known caustic of the pure Gaussian laser beam was simulated first without using the beam shaper. In figure 2 the result for ω_{fs} =2.5mm and a wavelength λ= 532nm is shown.
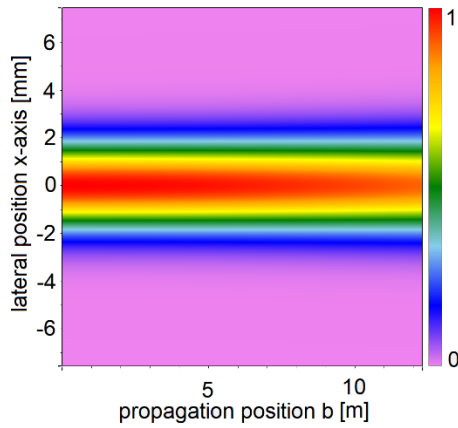

Fig. 2 Caustic of Gaussian beam in free space, with ω_{fs} =2.5mm λ= 532nm

The waist ω_{fs} determines the Rayleigh length z_{rfs} of the Gaussian beam in free-space [42]:

$$z_{rfs} = \frac{\pi \cdot \omega_{fs}^2}{\lambda} \qquad (2)$$

The Rayleigh length is the distance from the waist at which the width of the Gaussian beam increases by a factor of $2^{0.5}$, the peak intensity decreases by 50%, and the phase front of the Gaussian beam has the strongest curvature [42]. For the simulated setup with ω_{fs} =2.5mm and a λ= 532nm the Rayleigh length z_{rfs} of the Gaussian beam in free-space is 36.908m.

If the beam shaping element is positioned at the location of the waist ω_{fs} (distance a = 0) the caustic from figure 3 can be observed. A clearly changed propagation behavior can be seen after the introduction of the diffractive structure. In addition, two positions can be identified along the direction of propagation, in which Top-Hat profiles can be identified. For the setup used, the Top-Hat profile shown in figure 4a is observed at z_{2TH}=5.376m and the Top-Hat profile shown in figure 4b is observed at z_{1TH}=8.853m. If you look at increased distances, a further homogenization of the profile can be seen from about 100m. A clear position as with the other two profiles cannot be defined for this profile, whereby homogenization is fully developed from approx. 150m (z_{zTH}), figure 4c. It can be seen that the Top-Hat profiles show slight

intensity peaks. The different Top-Hat profiles can be distinguished by the number of sub-peaks. The 2TH profile has 4x4 peaks, the 1TH has 3x3 peaks and the zTH has 2x2 peaks. If the distances z_{2TH}, z_{1TH}, z_{zTH} are set in relation to the Rayleigh length z_{rfs}, a fixed relation can be seen. The results shown in table 1 apply in general, regardless of size of waist ω_{fs} and wavelength λ.
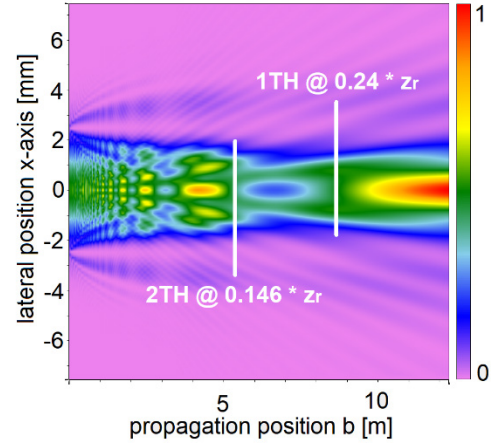

Fig. 3 Caustic of shaped beam in free space, with ω_{fs} =2.5mm, s= ω_{fs}, λ= 532nm

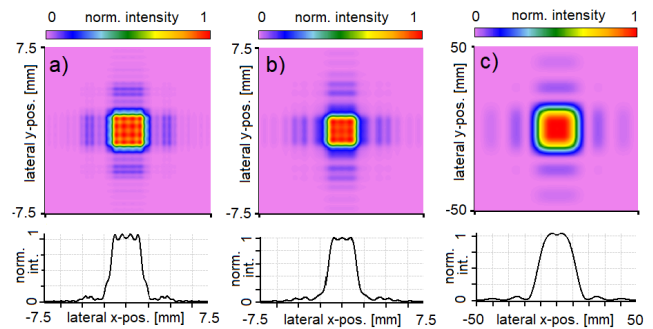**Fig. 4** Generated Top-Hat profiles in free space, with ω_{fs} =2.5mm, s= ω_{fs}, λ= 532nm, a) 2TH profile, b) 1TH profile, c) zTH profile

Table 1   Features for free-space Top-Hats

Top-Hat	shortcut	peaks	pos. [z_{rfs}]	FWHM [$2\omega_{fs}$]	$1/e^2$ [$2\omega_{fs}$]
2. order	2TH	4x4	0.146	0.58	0.8
1. order	1TH	3x3	0.24	0.54	0.74
0. order	zTH	2x2	≈ 4	4.76*	6.16*

* @ $4z_{rfs}$

These results show, that different Top-Hat profiles can be generated using the beam shaping element even without focusing optics. The size of the 2TH and 1TH profiles is about 20-25% smaller than the ω_{fs} of the Gaussian input beam. The size of the zTH profile is significantly further away than 2TH and 1TH and is therefore significantly larger, about 5 times larger than ω_{fs} of the Gaussian input beam.

The more general case with a ≠ 0 is considered in the following section. According to Fig. 1 the laser beam propagates the distance a from the waist to the beam shaper. It should be noted that the radius of the beam at the location of the beam shaper ω(a) must remain constant as parameter a increases. According to [42], the following applies to the determination of ω(a):

$$\omega(a) = \omega_{fs}\sqrt{1 + \left(\frac{a}{z_{rfs}}\right)^2} \tag{3}$$

In figure 5 the influence of distance a on the free space propagation of the shaped beam is shown. With a = 0, ω(a) = ω_{fs} =0.5mm, λ= 532nm the caustic shown in figure 5a is realized. If you compare figure 5a with figure 3, you can see the same caustic, whereby the adjusted scaling of image must be observed. According to the equation 2 and the lower Rayleigh length, the corresponding value of the z-axis (direction of propagation) is lower by a factor of $(2.5mm/0.5mm)^2 = 25$.

With a=0, the phase front is flat at the location of the beam shaper. If the distance a is now increased and ω(a) is kept at 0.5mm, ω_{fs} must decrease according to equation 2 and 3. Due to the increase in a, the phase front at the location of the beam shaper becomes increasingly curved. The curvature is strongest when the beam shaping element is positioned at the Rayleigh length z_{rfs} of the reduced waist radius ω_{fs}.

This relation is given by the following set of parameters: ω_{fs}=353.55μm, z_{rfs}=a=738.1mm, ω(a)=√2*ω_{fs}=0.5mm. The resulting caustic is shown in figure 5b.
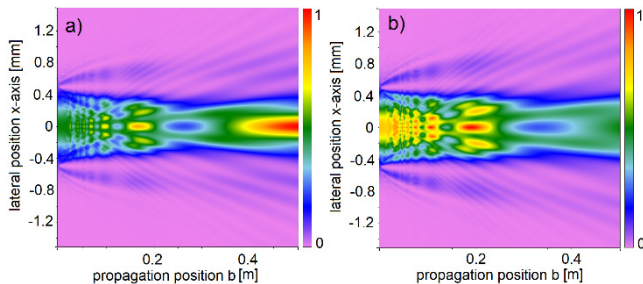
Fig. 5 Caustic of shaped beam in free space for λ= 532nm, a) a = 0, ω_{fs} = ω(a) = 0.5mm, s= ω_{fs}, b) a= z_{rfs}=738.1mm, ω_{fs} = 0.3536mm, ω(a) = 0.5mm, a = 0, s= ω(a)

A comparison of the two caustics shows only minor deviations. The position of the Top-Hat profile is about 20% further away, the size of the Top-Hat profile increases by about 20%. Therefore, the distance a should not play a bigger role for the further consideration.

In this section the free space propagation of the shaped beam is analyzed. The results presented can be used to homogenize laser beams in the one to two-digit meter range. This could possibly be advantageous for LIDAR in autonomous driving or other metrological methods.

3.1.2 Propagation of focused shaped beam

In order to generate Top-Hat sizes in the μm range, the laser beam formed by the shaping element must be focused. In this section, the previous setup is therefore expanded by

focusing optics. In addition, the distance b (between beam shaper and focusing optic) is introduced. Results with a = b = 0 and ω = ω_{fs} already published in [38] are summarized again, which are necessary for further understanding in the context of the paper. The setup used in the simulation is shown in figure 6.
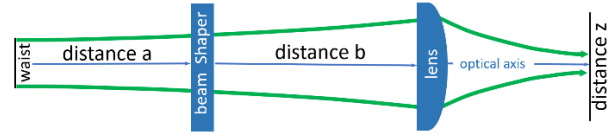

Fig. 6 Simulation setup for focused beam

For the focal area of interest, the caustics of the unshaped, focused Gaussian beam were first determined. A laser beam with ω = 2.5mm at 532nm was used. The focal length f of the focusing optic is 80mm. The distances a and b are zero. The resulting caustic is shown in figure 7.
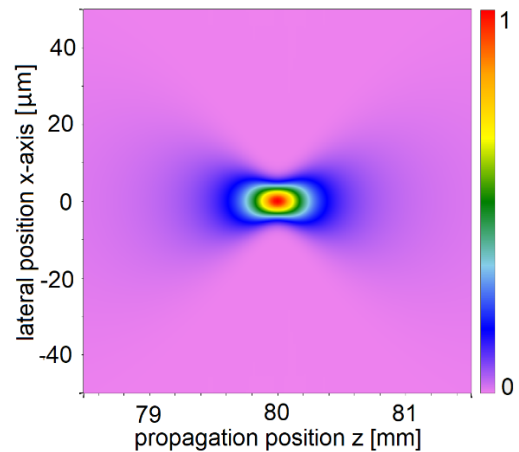

Fig. 7 Caustic of focused Gaussian beam along z axis

Figure 8 shows the phase distribution of the focused beam along the caustic. In the area of the focal plane at z=80mm, the intensity of the beam in the edge area of the x-axis (+/- >20μm) is almost zero. This leads to numerical artifacts when calculating the phase in these areas. For this reason, these areas that are of no interest to the application have a gray background.
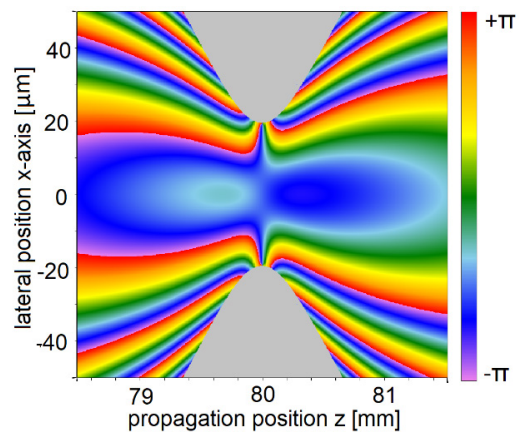

Fig. 8 Phase distribution along caustic of focused Gaussian beam

Finally, Figure 9a shows the two-dimensional Gaussian intensity distribution of the beam waist at the focal plane z=80mm. Figure 9b shows the phase front of the beam at the waist. A homogeneous phase distribution can be seen. In addition, the plane of oscillation of the linearly polarized beam is shown in both figures.
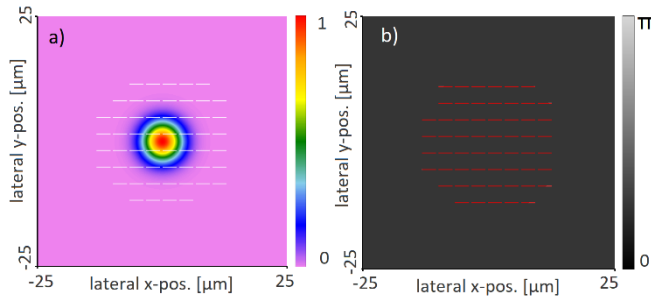

Fig. 9 Intensity (a) and phase distribution (b) of focused Gaussian beam at beam waist at z=80mm. Horizontal line indicates direction of linear polarization

The numerical aperture NA of the focused beam is calculated by:

$$NA = \frac{\omega}{f} \tag{5}$$

In the focal plane the beam shows the smallest width, called waist. The numerical aperture NA determines the waist ω_f of a focused Gaussian beam with an ideal beam quality M² =1:

$$\omega_f = \frac{\lambda}{\pi \cdot NA} \tag{6}$$

The waist ω_f determines the Rayleigh length z_{rf} of the focused beam:

$$z_{rf} = \frac{\pi \cdot \omega_f^2}{\lambda} \tag{7}$$

Taking a cross-section from figure 7, along z axis, with x=y=0 shows the variation of peak intensity along the optical axis for the propagating beam. As typical for focused Gaussian beams, the highest peak intensity is located in the focal plane at 80mm (Fig. 10).
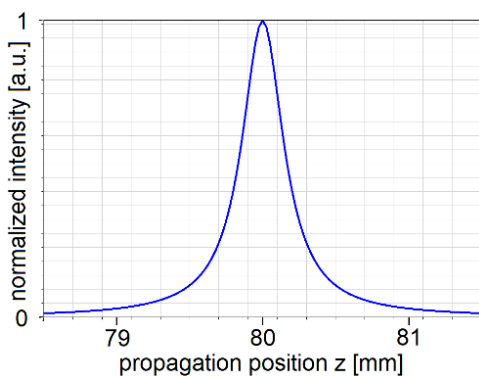

Fig. 10 Cross-section along optical axis z for focused Gaussian beam, x=y=0

By combining the Gaussian input beam with the beam shaper, the caustic of the focused beam is changed as shown in figure 11.
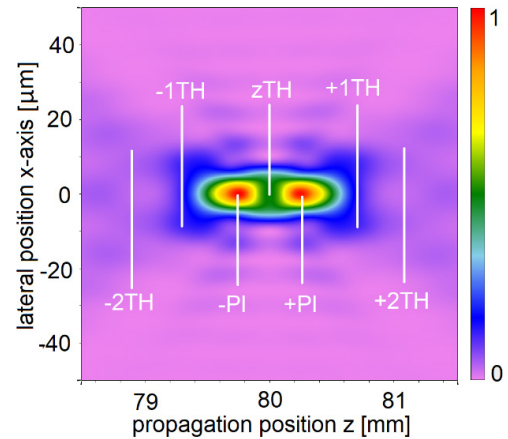

Fig. 11 Caustic of focused shaped beam along z axis (s= ω=2.5mm, f=80mm, NA=0.03125, λ = 532nm)

Figure 12 shows the phase distribution of the focused beam along the caustic when the beam shaping element is used. Compared to the phase distribution of the unshaped Gaussian beam from figure 8, only a small change can be seen.
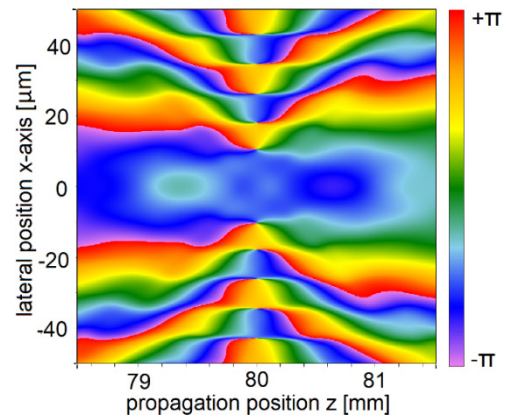

Fig. 12 Phase distribution along caustic of focused shaped

Figure 13 shows the changed intensity and phase distribution in the focal plane at z=80mm due to the beam shaping. The intensity distribution from figure 13a agrees with that from the free space propagation in the far field (figure 4c). One can see the square and rectangular intensity ranges separated by zero crossings. The phase distribution shown in figure 13b shows that the phase changes suddenly between zero and Pi as the intensity crosses zero. After such a zero crossing, the amplitude oscillates locally offset by 180°, which is indicated by the different colors of the horizontal lines. However, compared to the direction of polarization of the unshaped Gaussian beam (figure 9b), the beam-shaping element does not affect the type of polarization or its orientation in space, which is indicated by the orientation of the horizontal lines.
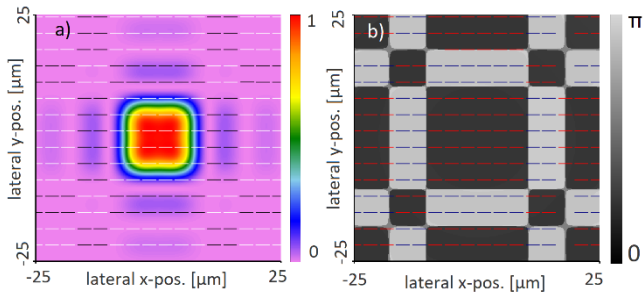
Fig. 13 Intensity distribution (a) and phase distribution (b) of focused shaped

A cross-section of figure 11, along the optical axis z, with x=y=0 shows that the peak intensity on the optical axis varies. The variation of the peak intensity on the optical axis along the axis z is shown in figure 14. It can be seen that the highest peak intensity is no longer in the focal plane as with the Gaussian beam, but is in front of and behind it (±1PI). Also, the positions of two second order Top-Hats (±2TH), of the two first order Top-Hats (±1TH), as well as of the zero order Top-Hat (zTH) are shown.
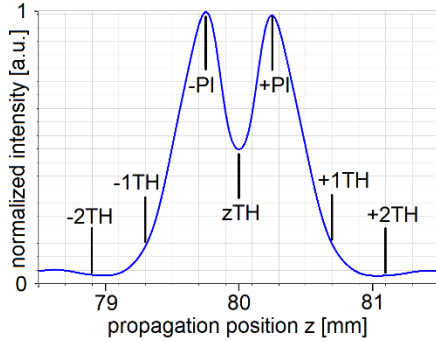

Fig. 14 Cross-section along optical axis z (x=y=0) for shaped beam according to Fig. 11, relative intensity levels for characteristic profiles are indicated

For values of NA above 0.3, the caustic can be considered to be symmetrical. Therefore, in such cases, the characteristic profiles mentioned above are arranged in pairs, symmetrically around the focal plane. The normalized cross-sections of the characteristic intensity profiles and the corresponding unshaped Gaussian focal spot are shown in figure 15.
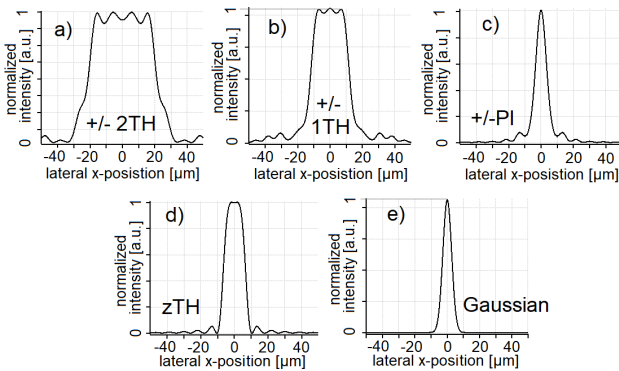

Fig. 15 Intensity cross-section of characteristic profiles, a) ± second order Top-Hats (±2TH), b) first order Top-Hats (±1TH), c) peak intensities (±PI), d) zero-order Top-Hat (zTH) at focal plane, e) unshaped Gaussian focal spot

The size of the characteristic profiles and their position depend only on the NA and the wavelength λ. Table 2 shows the benchmark values for the relative intensity, location normalized to the Rayleigh length z_{rf}, the width at FWHM normalized the FWHM of the unshaped Gaussian focal spot and the width at $1/e^2$ normalized to the radius ω_f of the unshaped Gaussian focal spot, respectively.

Table 2   Features of characteristic profiles

Profile	relative intensity	Rel. location [z_{rf}]	FWHM [Gaussian FWHM]	width $1/e^2$ [$2\omega_f$]
± 2TH	0.04	6.87	6.76	5.51
±1TH	0.12	4.20	3.84	3.15
±PI	1	1.44	1.23	1.28
zTH	0.5	-	2.06	1.55

3.1.3 Symmetry of caustic

The maximum value of the peak intensity (-PI) in front of the focal plane can be defined as IPI, and the maximum value of the relative peak intensity (+PI) behind the focal plane as BPI. In this case the homogeneity hp of both peaks can be calculated as follows [38]:

$$h_p = 1 - \frac{IPI - BPI}{IPI + BPI} \qquad (8)$$

If h_p is close to 1, the propagation behavior is symmetrical with respect to the focal plane. The symmetry of the caustic of the shaped focused beam shown in the previous section can be broken by two parameters. The first parameter is the NA of the focused beam. For values of NA less than 0.3, the symmetry decreases with NA→ 0. With NA=0, the zero-order Top-Hat is the far-field profile according to Fig. 4c and every profile behind vanishes. The behavior of the broken symmetry is shown in figure 16a using the example of a focused beam with ω= 0.75mm, λ = 532nm, f= 80mm, NA = 0.0094 and a=b=0. In this case the value of h_p is 1.15.

By increasing the parameter b, it can be observed a free space propagation between the beam shaper and focusing optic according to section 5.1. Due to this free space propagation, parts of the caustic do not reach the focusing optic and are therefore no longer available to the caustic of the focused beam. As a result, parts of the caustic disappear in front of the focal plane, causing the asymmetry to tilt in the opposite direction. This relationship is shown in figure 16b for the parameter set ω= 0.75mm, λ = 532nm, f= 80mm, NA = 0.0094, b=166mm and a=0. In this case the value of h_p is 0.86. Therefore, when varying from b= 0 to b=166mm, the value hp=1 must be exceeded. This happens for this special case with NA=0.0094 at b ≈ 70mm. The resulting caustic for the parameter set ω= 0.75mm, λ = 532nm, f= 80mm, NA = 0.0094, b = 70mm and a=0 is shown in Fig. 16c.
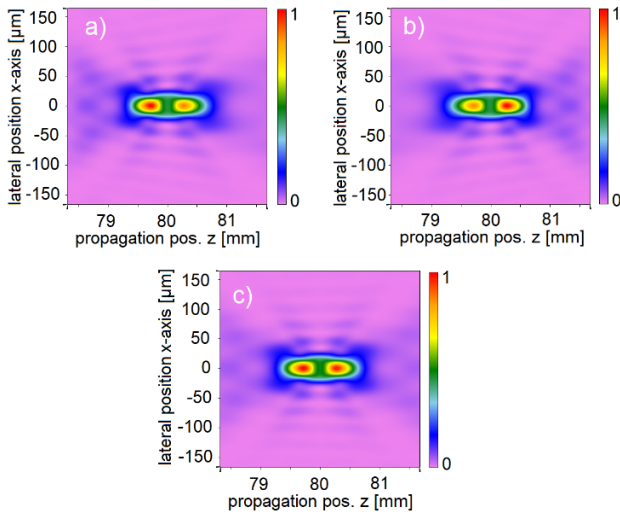
Fig. 16 Caustic of shaped beam along z axis, ω= 0.75mm, λ = 532nm, f= 80mm, NA = 0.0094, a) b=0mm, b) b=166mm, c) b=70mm

It is obvious that the influence of the value of b according to section 5.1 becomes significantly less sensitive with increasing radius ω_{fs} of the Gaussian beam, because according to equation 2 there is a quadratic dependency. And it can be assumed that there is a certain combination of NA and b that results in a value for h_p close to 1 and produces a symmetric propagation behavior. Based on this assumption, a parametric study was performed to obtain the h_p value as a function of NA and b. In order to get a more general relation, one can express the parameter b in units of the Rayleigh length z_{rfs} of the unfocused beam with the waist radius of ω_{fs}. The results of this parametric study are shown in figure 17.

From the figure, it is possible to derive the h_p value as a function of NA and b. Where b is specified in the unit of the Rayleigh length of the free space beam.
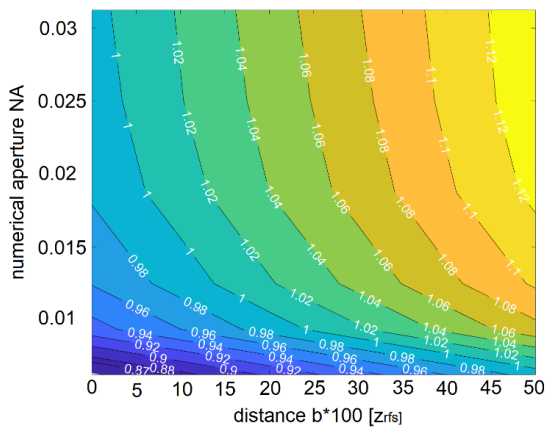

Fig. 17 Map for the homogeneity h_p and its dependence on NA and b

If you are close to the line with h_p = 1 with your parameter combination, then there is a symmetrical propagation behavior of the caustic, the two peaks $\pm$PI have identical intensity values (Fig. 16c) and the relationships shown in table 2 are valid. If you have an h_p value from the yellowish range, the intensity value of (-PI) is greater than that of (+PI), corresponding to Fig.16a. The caustic is unsymmetrical and the

propagation behavior after the focal plane is stretched compared to the propagation behavior before the focal plane. The position and size of the Top-Hat profiles 2TH and 1TH in particular has changed significantly depending on the hp value. If you have an h_p value in the bluish range, the opposite is the case, corresponding to Fig.16b.

As shown in section 5.1, the parameter a has no significant influence on the free-space propagation (Fig. 5), so that there is no appreciable influence on h_p by the parameter a, table 3. This is because the caustic in front of the focusing optics depends only slightly on parameter a and is essentially determined by parameter b.

Table 3 Influence of parameter a on h_p

ω_{fs} [μm]	a [mm]	$\omega(a)$ [μm]	b [mm]	f [mm]	h_p
353.5	738.16	500	0	80	1.38
353.5	738.16	500	70	80	1.01
500	0	500	0	80	1.36
500	0	500	70	80	1

3.1.4 Symmetry for enhanced depth of focus

The caustic can be stretched or compressed overall by changing the parameter s. This also changes the positions of the characteristic profiles $\pm$ (2TH, 1TH, PI). If the value s > ω, the zTH and the $\pm$2TH profiles disappears and the peaks $\pm$PI are closer together (Fig. 18).

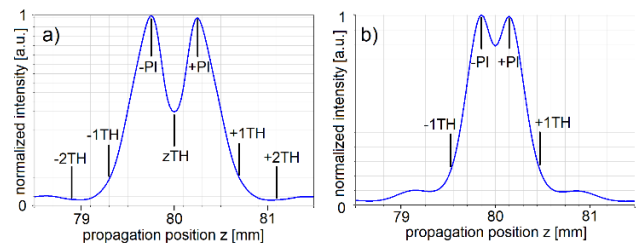**Fig. 18** Cross-section along optical axis z (x=y=0) for FBS shaped beam, ω=2.5mm, f=80mm, NA=0.03125, λ = 532nm, a) s= ω, b) s=1.25ω, relative intensity levels for characteristic profiles are indicated

As the s value increases, the peaks merge and it is possible to obtain an increased depth of field compared to Gaussian beam (Fig. 19), while footprint remains nearly Gaussian.
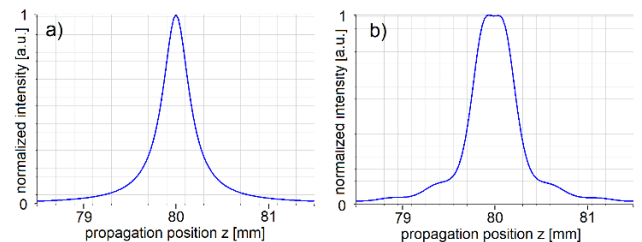

Fig. 19 Cross-section along optical axis z (x=y=0), ω=2.5mm, f=80mm, NA=0.03125, λ = 532nm, a) unshaped Gaussian, b) shaped beam with s=1.5ω

In order to achieve the best possible homogeneity, the findings from sections 5.1 and 5.2 must be taken into account while varying s, since only a value of h_p close to 1 allows the increase in depth of field.

3.1.5 Influence of NA and b on size and location of higher order Top-Hat profiles

As shown in section 5.3, some combinations of NA and b can introduce an asymmetry into the caustic, which changes the position and size of the Top-Hat profiles compared to the values in table 2. This can be used in a targeted manner to increase the possibilities of achieving different Top-Hat sizes with a single beam shaping element. This is exemplified for the -2TH profile shown in Fig. 20. With larger values of b, even more pronounced changes in Top-Hat size can be achieved. A detailed documentation of all possible variants would go beyond the scope of this publication.
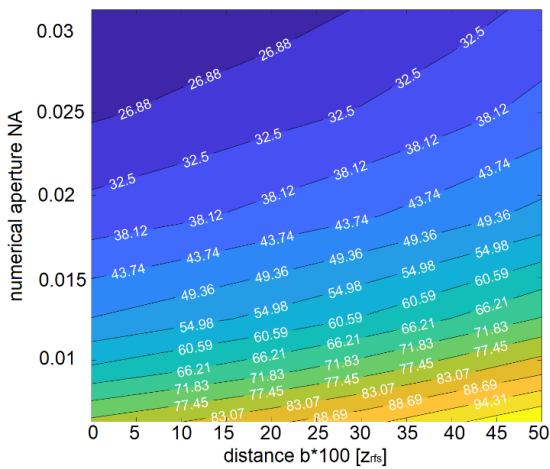
Fig. 20 Map for the size of -2TH profile and its dependence on NA and b

3.1.6 Adaption of generated Top-Hat sizes and geometry

Another way to increase the flexible use of the beam shaping element is to consider the x- and y- axes separately. In this way, different x- and y-positions of the caustic can be superimposed. So, it is possible for example to overlay the zTH profile of the x-axis with the -2TH profile of the y-axis to get a rectangular Top-Hat profile.

For this, the x- and y- axis must have different focal lengths. In the simplest case, it would be conceivable to combine a cylindrical optic with a spherical optic. About the distance between the cylinder optic and the spherical optic, the focal length could be set specifically for one axis. In this case, a very detailed consideration regarding the focal lengths that can be achieved and the resulting positions of the characteristic profiles +/-(2TH, 1TH, PI) and zTH must be made in advance.

A much more flexible method would be to use a cylinder telescope with a magnification scale of 1. Here you can generate an additional refractive power by means of a non-ideal collimation after the telescope and place the position of the characteristic profile for one axis arbitrarily on a characteristic profile of the unaffected axis. In addition, a cylinder telescope can also have a different magnification scale or a zoom function with a variable magnification scale. Of course, two cylindrical telescopes rotated by 90° can also be combined.

The concept is shown in Fig. 21. In this example, the x-axis only passes through the spherical lens for focusing. The y-axis, on the other hand, is widened by a cylinder telescope and a slight additional refractive power due to the non-optimal collimation. This allows the different positions to be superimposed.
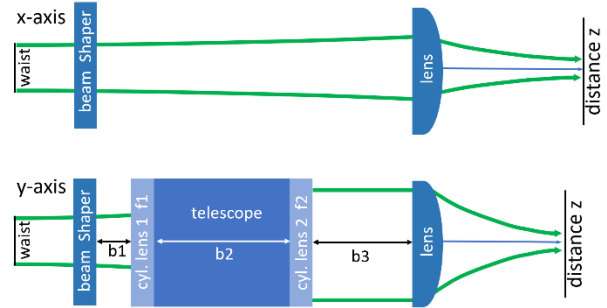
Fig. 21 Schematic of optical setup to adjust Top-Hat size and geometry

Simulations were carried out based on figure 21. For this purpose, ideal cylindrical lenses (thickness 0mm) for the y-axis were used. Lenses with a focal length of f_1=-100mm and f_2=200mm were positioned one after the other at a distance b_2 of 100mm to realize a cylinder telescope with a magnification of 2. With b_2=100mm there is an ideal collimated beam. The input beam of the laser has a radius of ω_{fs}=0.75mm, the distance a is zero. The distances b_1 (beam shaper | telescope) and the distance b_3 (telescope | spherical lens) are also zero. The collimation of the y-axis and thus the position of the characteristic profiles can be controlled via the distance b_2.

The resulting profiles in the focal plane of the spherical lens with f= 80mm for different values of b_2 are shown in figure 22. It should be clear that the zTH Top-Hat profile is generated for the x-axis in the focus of the spherical lens and the other characteristic profiles are superimposed on this profile by changing the collimation of the y-axis. Inserting the cylinder telescope creates an additional distance between the beam shaper and the focusing optics. This affects the symmetry of the caustics. In addition, the NA of the y-axis is changed, which also affects the caustics. Whether the findings from section 5.3 – 5.5 can be transferred one-to-one to the use of a telescope is not the subject of this work. However, the basic behavior is given. The following table 4 gives an overview of the superimposed profiles shown in figure 22.
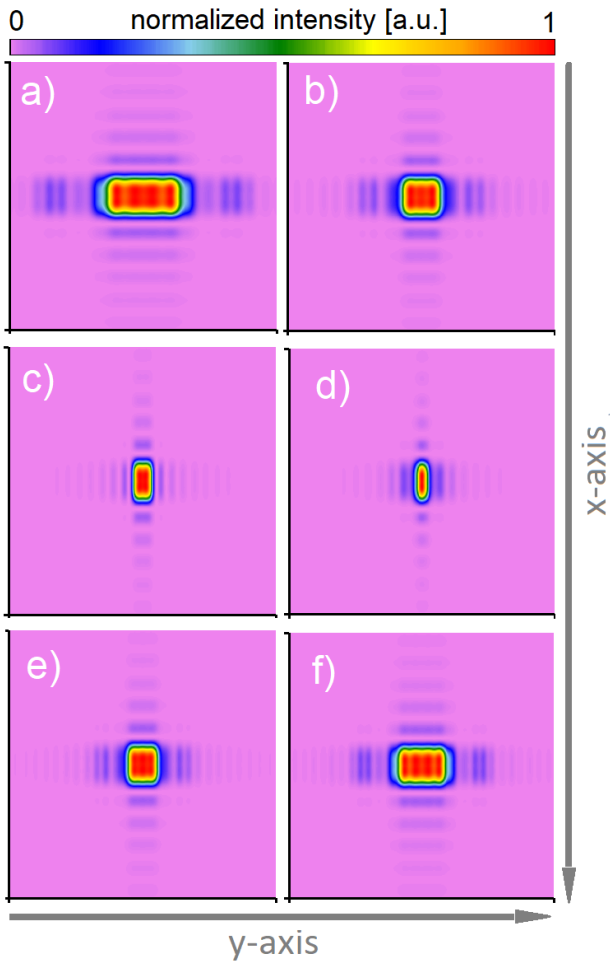
Fig. 22 Different profiles generated in the focal plane of the spherical lens by varying the parameter b2, each frame has a size of 50x50µm, a) b2=74.25mm, b) b2=85.75mm, c) b2=100mm (collimated), d) b2=95mm, e) b2=111mm, f) b2=117mm

Table 4 Overview superimposed profiles

Figure	b2 [mm] y-axis	profile x-axis	profile y-axis
22a	74.25	zTH	-2TH
22b	85.75	zTH	-1TH
22c	100mm (collimated)	zTH	zTH
22d	95.00	zTH	+PI
22e	111.00	zTH	+1TH
22f	117.00	zTH	+2TH

3.1.7 Considering other geometries for phase structure

One-dimensional phase structures which enable the generation of a one-dimensional homogenized profiles have already been described in the literature [43]. The cross section along the homogenized intensity profile is similar to that of the zTH profile. As part of the work on two-dimensional beam shaping described here, it was also examined whether the relationships described above also apply to one-dimensional structures.

In summary, with one-dimensional beam shaping, there are Top-Hat profiles in front of and behind the focal plane, similar to the +/- 2TH and +/- 1TH profiles. The concepts from sections 5.3, 5.5 and 5.6 can also be applied. The profiles of the peaks +/-PI can also be seen, but in the case of one-dimensional phase structures their intensity is not higher than the intensity in the focal plane. If you create a cross-section similar to figure 10 or 14 for the one-dimensional case, it will resemble figure 10. Thus, the concept of extended depth of field is not transferrable to the one-dimensional case.

3.2 Experimental results

The setup shown in figure 23 was used for the experiments. A cw - Nd:YAG laser with intracavity SHG was used as the light source, wavelength $\lambda = 532$nm, power p = 5mW. The beam was then expanded using a motorized zoom telescope developed by Topag Lasertechnik. After the telescope the laser beam was directed via the mirrors M1 and M2 to a CinSquare measuring device from Cinogy, model: CS-300h, to determine the beam quality M² of the laser beam for different magnification.

After checking the beam quality, the mirror M1 was removed, different optical setups were realized and the resulting light distributions were detected with a WinCamD-LCM camera.
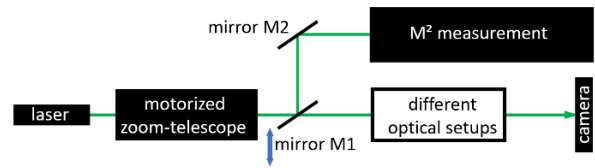

Fig. 23 Scheme of the experimental setup

The beam quality was measured up to a 4-fold expansion, resulting in a beam diameter of 3.6 mm. The beam quality M² was < 1.05 for all measurements. The ellipticity was always in the range of 0.96. Finally, a beam diameter of 3mm @1/e² was set behind telescope for further investigations. The resulting profile is shown in figure 24.
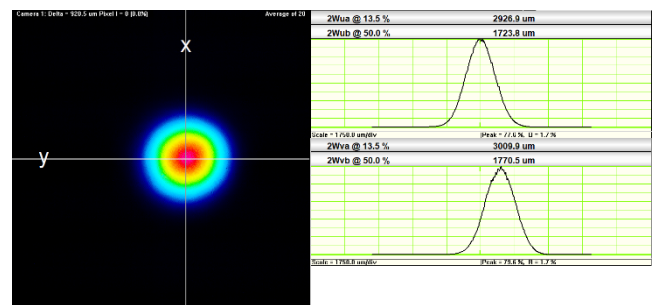

Fig. 24 Beam profile behind the telescope

3.2.1 Extend depth of focus

For the experimental verification of the findings from sections 5.1, 5.3 and 5.4, the setup shown in figure 25 is positioned behind the telescope from figure 23. A self-developed objective with a focal length of 88mm was used for focusing. This ensured a good focusing property.
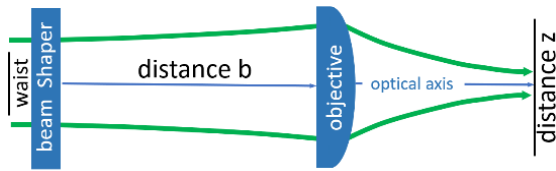
Fig. 25 Scheme of the optical setup behind spherical telescope for enhanced depth of focus

With ω=1.5 mm and b=0, the resulting NA=0.017 already leads to a high homogeneity h_p. With b=100mm = $0.007 \cdot z_{rfs}$, h_p can be optimized to reach a value close to one. The maximum intensity for different positions was determined along the caustic of the focused beam. The results are shown in figure 26. First, a diffractive structure with s=ω was used. The resulting intensity profile is shown in figure 26a. A high value of h_p close to 1 can be seen. In addition, the results show a relative intensity of zTH to ±-PI of 0.52, which corresponds to the value from table 2 with a small deviation around 5%.

Replacing the beam shaper by an element with a diffractive structure with s=1.5ω results in the intensity profile shown in figure 26b. The high homogeneity of the +/-PI peaks still can be seen, but according to section 5.4 the peaks are almost merged, which means that the effective depth of focus can be increased.
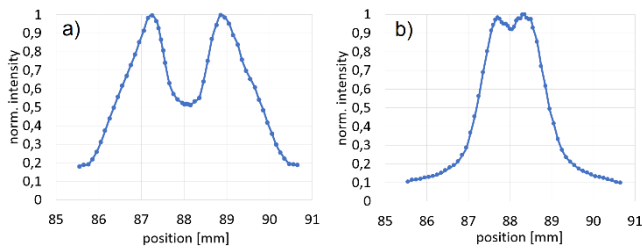

Fig. 26 Measured peak intensity along optical axis z, ω=1.5mm, f=88mm, NA=0.017, b=100mm, λ = 532nm a) s=ω, b) s=1.5ω

3.2.2 Adaption of generated Top-Hat sizes and footprints using cylindrical telescope

In order to generate homogenized beam profiles with different sizes and geometries, the optical system shown in figure 27 was placed behind the spherical telescope. The optical system consists of a beam shaper for 3mm Gaussian input beam, a cylindrical lens with f = 400mm (Thorlabs LJ1363RM-A), a cylindrical lens with f = -200mm (Thorlabs LK1069RM-A) and a spherical lens with f = 250mm (Eksma 110-0235E|AR532) for focusing. The cylindrical lenses form a cylindrical telescope for the y-axis with a reduction factor of 2. With b_2 =198mm, the cylindrical telescope delivers a collimated output beam with a diameter of 3mm for the x-axis and a diameter of 1.5mm for the y-axis. The resulting output beam is shown in figure 28.
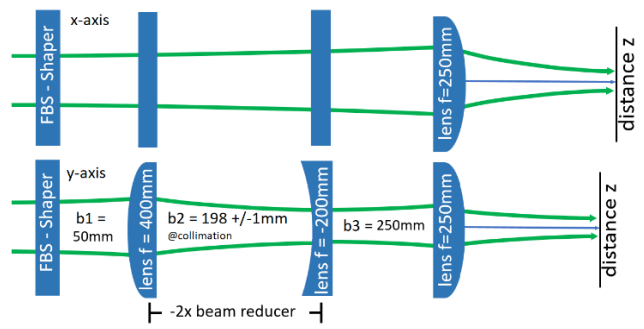

Fig. 27 Scheme of the optical setup behind spherical telescope for variation of Top-Hat geometry
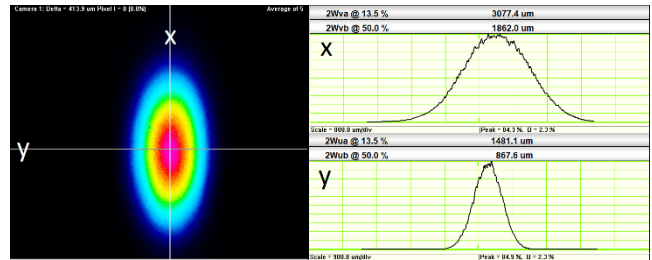

Fig. 28 Beam profile behind the cylindrical telescope, no FBS element in beam path

If the camera is positioned in the focal plane of the spherical lens, the Top-Hat distribution shown in figure 29a is obtained. The zTH profile (2 peaks, see Table 1) can be seen for both axes, whereby the width of the profile differs for the two axes and therefore has a rectangular footprint. The ratio of the edge length corresponds to that of the reduction factor of the cylindrical telescope.

If the distance b_2 changed that there is no longer any collimation, the effective focal length for the y-axis is changed, so to speak. In this way, different profiles can be generated for the y-axis at the fixed location of the camera and superimposed on the zTH profile of the x-axis. In figure 29b this effect is for the combination zTH | 1TH and in figure 29c for the combination zTH | 2TH shown.

Clearly, the camera can also be positioned outside the focal plane of the spherical lens, so that the zTH profile is no longer recognizable for the x-axis. For example, it is possible to position the camera at the position of the -2TH profile on the x-axis. In this case, too, the different characteristic profiles of the y-axis can be superimposed on the -2TH profile of the x-axis via the distance b_2. In figure 30a this effect is for the combination -2TH | zTH, in figure 30b for the combination -2TH | Pi and in figure 30c for the combination -2TH | 1TH shown.

The experimental results confirm the theoretical considerations from section 5.6 and show the flexible use of the beam shaping element.
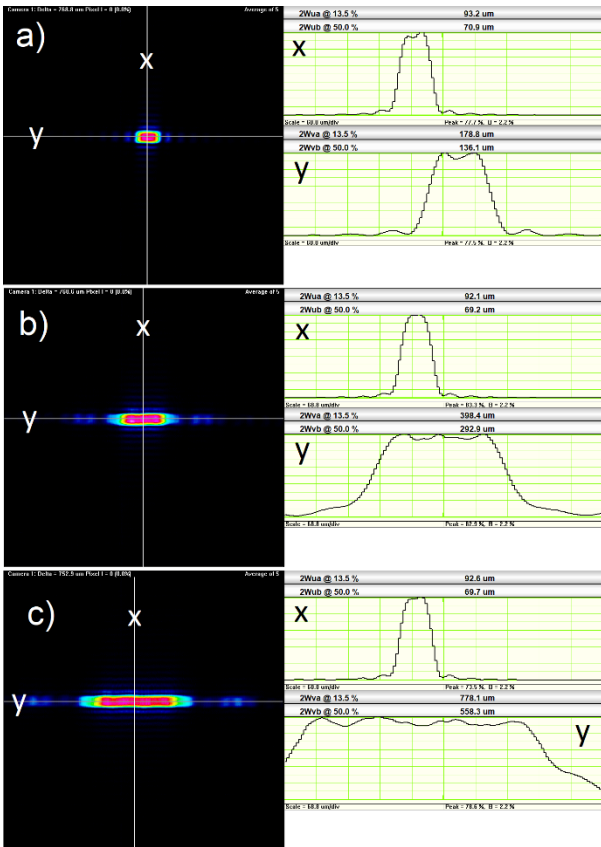
Fig. 29 Measurements of superimposed beam profiles in the focal plane, a) zTH (x-axis) | zTH (y-axis), b) zTH (x-axis) | 1TH (y-axis), c) zTH (x-axis) | 2TH (y-axis)
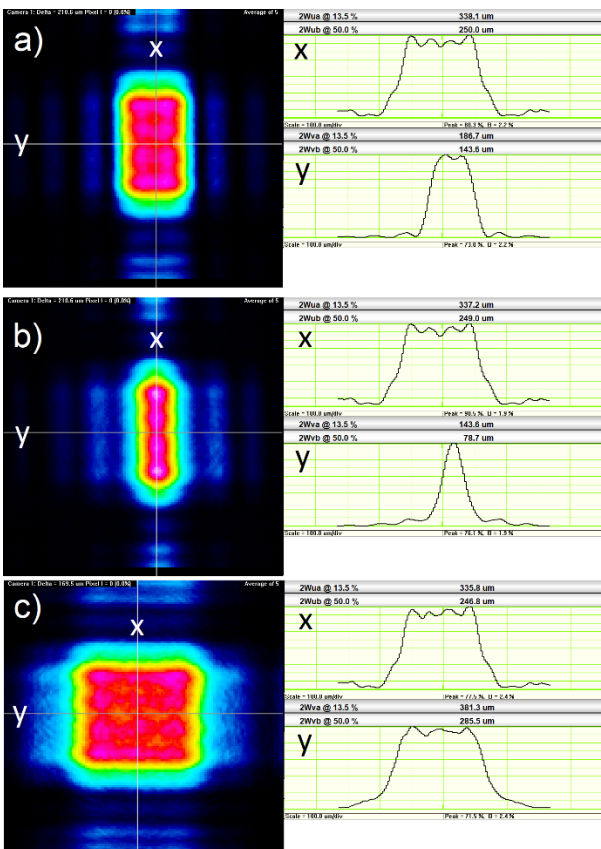

Fig. 30 Measurements of superimposed beam profiles outside the focal plane, a) -2TH (x-axis) | zTH (y-axis), b) -2TH (x-axis) | PI (y-axis), c) -2TH (x-axis) | 1TH (y-axis)

4. Conclusion

The study examined how the free space propagation between a beam shaping element for Top-Hat generation and the focusing optics affects the beam shaping result used in laser micromachining. The distance between the beam shaping element and the focusing optics can influence the position and size of the achievable Top-Hat profiles. For certain positions there is a symmetrical caustic of the focused beam. If this is the case, the beam shaping property can be used by adjusting the optical setup to increase the depth of field of a Gaussian profile. In addition, concepts were presented that allow different Top-Hat geometries to be achieved with one beam shaping element.

References

[1] Y. Yao, H. Chen, and W. Zhang: Int. J. Adv. Man. Tech, 26, (2005) 598.
[2] Q. Wang, A. Smanta, S. Shaw, H. Hu, and H. Ding: Appl. Surf. Sci., 507, (2020) 145136.
[3] J. Zhang, S. Tao, B. Wang, and J. Zaho: Proc. SPIE, Vol. 9735, (2016) 973514.
[4] J. Linden, S. Cohen, Y. Berg, Z. Kotler, and Z. Zalevsky: J. Laser Micro Nanoengin., 16, 1, (2021) 14.
[5] A. Lemke, D. Ashkenasi, and H.J. Eichler: Phys. Procedia, 41, (2013) 769.
[6] B. Neuenschwander, B. Jaeggi, M. Schmid, G. Hennig: Phys. Procedia, 56, (2014) 1047.
[7] G. Raciukaitis: JSTQE, 27, 6, (2021) 1100112.
[8] D. Mikhaylov, T. Kiedrowski, and A.F. Lasagni: Proc. SPIE, 10906, (2016) 1090615.
[9] C. Lutz, G.L. Roth, S. Rung, C. Esen, and R. Hellmann: J. Laser Micro Nanoengin., 16, 1, (2021) 62.
[10] D. Flamm, D.G. Großmann, M. Jenne, F. Zimmermann, J. Kleiner, M. Kaiser, J. Hellstern, C. Tillkorn, and M. Kumkar: Proc. SPIE, Vol. 10904, (2019) 109041G.
[11] D. Dudutis, R. Stonys, G. Raciukaitis, and P. Gecys: Opt. Express, 26, 3, (2018) 3627.
[12] A. Gillner, J. Finger, P. Gretzki, M. Niessen, T. Bartels, and M. Reiningshaus: J. Laser Micro Nanoengin., 14, 2, (2019) 129.
[13] R. Shi, S.A. Khairallah, T.T. Roehling, T.W. Heo, J.T. McKeown, and M.J. Matthews: Acta Mat., 184, (2020) 284.
[14] S.M.A. Noori Rahim Abadi, Y. Mi, F. Sikström, A. Ancona, and I. Choquet: IJTS, 166 (2021) 106957.
[15] S.P. Murzin, N.L. Kazanskiy, and C. Stiglbrunner: Metals, 11, (2021) 963.

[16] T. Häfner, J. Strauß, C. Roider, J. Heberle, and M. Schmidt: Appl. Phys. A, 124, 2, (2018) 111.

[17] J.W. Goodmann: "Introduction to Fourier Optics", 2nd ed., (McGraw-Hill: New York, NY, USA, 1996) p. 111

[18] F.M. Dickey and C.S. Holswade: "Laser Beam Shaping: Theory and Techniques", 1st. ed. (Marcel Dekker Inc.: New York, NY, USA, 2000) p. 82.

[19] A. Laskin and V. Laskin: Proc. SPIE, Vol. 8236, (2012) 82360D.

[20] F. Wyrowski and O. Bryngdahl: Rep. Prog. Phys., 54, (1991) 1481.

[21] F. Wyrowski: J. Opt. Soc. Am. A, 7, 6, (1990) 961.

[22] O. Ripoli, V. Kettunen, and H.P. Herzig: Opt. Eng., 43, 11, (2004) 2549.

[23] F. Wyrowski: Opt. Comm., 92, (1992) 119.

[24] H. Aagedal, M. Schmid, T. Beth, S. Teiwes, and F. Wyrowski: J. Mod. Opt., 43, 7, (1996) 1409.

[25] P.S. Salter and M.J. Booth: Light Sci. Appl., 8, (2019) 110.

[26] L. Kong, Y. Ma, M. Ren, M. Xu, and C. Cheung: Sci. Prog., 103, 1, (2020) 21.

[27] X. Su, P. Ji, K. Liu, D. Walker, G. Yu, H. Li, D. Li, and B. Wang: Opt. Express, 27, 13, (2019) 17979.

[28] R.E. Lee: "Ion-Beam Etching (Milling)", VLSI Electronics Microstructure Science, Volume 8, ed. by N.G. Einspruch and D.M. Brown, (Academic Press: Cambridge, MA, USA, 1984) 341

[29] J. Schmitt, C. Bischoff, U. Rädel, M. Grau, U. Wallrabe, and F. Völklein: Proc. SPIE, Vol. 9628 (2015) 96281P

[30] P.W. Leech: Vacuum, 55, (1999) 191.

[31] C. Bischoff, U. Rädel, U. Umhofer, and E. Jäger: Proc. SPIE, Vol. 8600, (2013) 860024.

[32] J. Jia, H. Fu, Z. Hou, H. Wang, Z. Wang, F. Dong, Z. Ni, and Z. Zhang: Spectrochimica Acta Part B, 163, (2020) 105747.

[33] C. Basler, A. Brandenburg, K. Michalik, and D. Mory: Sensors, 19, (2019) 4133.

[34] M. Wiegelmann, K. Dreisewerd, and J. Soltwisch: J. Am. Soc. Mass Spectrom., 27, (2016) 1952.

[35] M. El-Khoury, B. Voisiat, T. Kunze, and A. F. Lasagni: J. Laser Micro Nanoengin., 13, 3, (2018) 268.

[36] R. Raciukaitis, E. Stankevicius, P. Gecys, M. Gedvilas, C. Bischoff, E. Jäger, U. Umhofer, and F. Völklein: J. Laser Micro Nanoengin., 6, 1, (2011) 37.

[37] S. Rung, M. Rexhepi, C. Bischoff, and R. Hellmann: J. Laser Micro Nanoengin., 8, 3, (2013) 309.

[38] C. Bischoff, E. Jäger, U. Umhofer, A.F. Lasagni, and F. Völklein: J. Laser Micro Nanoengin., 15, 3, (2020) 178.

[39] K.J. Kasunic: "Laser Systems Engineering", (SPIE, 2016) p. 99

[40] Z. Wang, S. Zhang, O. Baladron-Zorita, C. Hellmann, and F. Wyrowski: Opt. Express, 27, 11 (2019) 15335.

[41] Z. Wang, O. Baladron-Zorita, C. Hellmann, and F. Wyrowski: Opt. Express, 28, 7, (2020) 10552.

[42] J. Alda: "Encyclopedia of Optical Engineering" ed. by R.G. Driggers (Publisher Marcel Dekker, Inc., 2003) 999.

[43] W.B. Veldkamp and C.J. Kastner: Appl. Opt., 21, (1982) 345.